

## NiFe<sub>2</sub>O<sub>4</sub>-Coated Activated Carbon Composite as a Cathode Material for Lithium–Sulfur Batteries

Riguang Cheng, Lixian Sun\*, Fen Xu\*, Yumei Luo, Chenchen Zhang, Yongpeng Xia, Sheng Wei, Yanxun Guan, Mengmeng Zhao, Qi Lin, Hao Li

Guangxi Key Laboratory of Information Materials, Guangxi Collaborative Innovation Center of Structure and Property for New Energy and Materials, School of Material Science and Engineering, Guilin University of Electronic Technology, Guilin, 541004, P. R. China

\*E-mail: [sunlx@guet.edu.cn](mailto:sunlx@guet.edu.cn), [xufen@guet.edu.cn](mailto:xufen@guet.edu.cn) or [1732211579@qq.com](mailto:1732211579@qq.com)

Received: 25 October 2019 / Accepted: 23 December 2019 / Published: 10 February 2020

Lithium–sulfur batteries are promising as next-generation rechargeable energy-storage devices because of their high energy density, low cost, and environmental friendliness. However, sulfur cathodes suffer from low specific capacity caused by the poor electrical conductivities of the active materials and fast capacity decay resulting from polysulfide dissolution/shuttling. Herein, we report a facile and low-cost method to solve these problems using an activated carbon (AC)–NiFe<sub>2</sub>O<sub>4</sub>/S hybrid material in which NiFe<sub>2</sub>O<sub>4</sub> is uniformly distributed on AC through a simple wet impregnation method. The AC–NiFe<sub>2</sub>O<sub>4</sub>/S material not only has a strong catalytic effect on sulfur reduction, but also provides strong binding sites to trap polysulfide intermediates. An AC–NiFe<sub>2</sub>O<sub>4</sub>/S electrode shows favorable electrochemical properties including stable reversible capacity (0.24% capacity decay per cycle at 0.1 C, retaining a capacity of 602.7 mAh g<sup>-1</sup> after 170 cycles; stable cycling at 0.5 C, retaining a capacity of 501.9 mAh g<sup>-1</sup> after 100 cycles), excellent rate performance, and fast electrochemical reaction kinetics compared with those of a reference AC/S electrode, which are attributed to the synergistic effects between NiFe<sub>2</sub>O<sub>4</sub> and AC.

**Keywords:** lithium–sulfur batteries; activated carbon; NiFe<sub>2</sub>O<sub>4</sub>

### 1. INTRODUCTION

With the rapid development of science and technology and the increasing demand for energy storage, it is important to search for low-cost and long-life lithium-ion batteries with high energy density. Lithium-ion batteries currently dominate the portable electronics market, but their theoretical energy density has reached its limitation. Lithium–sulfur (Li–S) batteries are considered a promising candidate for next-generation rechargeable batteries because of their great potential advantages. For example, the cathode material in Li–S batteries is sulfur, which is inexpensive, abundant, environmentally benign,

and has a high energy density [1-4]. These features of sulfur make Li-S batteries conducive to efficient, long-term stable energy storage. However, major challenges associated with Li-S batteries currently limit their practical applications, including (i) poor electronic and ionic electrode rechargeability and limited rate capability caused by the insulating nature of sulfur species and the formation of solid reduction products ( $\text{Li}_2\text{S}$  and  $\text{Li}_2\text{S}_2$ ); [5, 6] (ii) The shuttle mechanism occurs because the soluble polysulfides formed at the cathode are transported to the anode, where they are reduced to lower polysulfides that are transported back to the cathode, generating various dissolved polysulfides  $\text{Li}_2\text{S}_n$  ( $3 \leq n \leq 6$ ) [7, 8] in the electrolyte, which results in the shuttle mechanism displaying low Coulombic efficiency [9]; (iii) polysulfide dissolution results in large volumetric changes ( $\sim 80\%$ ), leading to destruction of the electrode structure during charging and discharging reactions [10].

To date, various strategies have been developed to improve the material structure of sulfur electrodes. Numerous nanomaterials such as carbon nanotubes, carbon nanospheres, carbon nanofibers, graphene, and, meso-/microporous carbons have been added to sulfur by chemical assembly and physical mixing to increase its electrical conductivity [11-14]. Although carbon materials generally have high electrical conductivity, they are non-polar and have a weak affinity with polar polysulfides.[15] Therefore, metal oxides and chalcogenides are used in electrodes because their strong binding to polysulfides leads to high Coulombic efficiency and cycling stability.[16-20] In particular, typical polar metal compounds (M-X, X: O, S, N, C, P, etc.) readily adsorb polysulfides [21-24].

Herein, we use  $\text{NiFe}_2\text{O}_4$  nanoparticles as an electrocatalyst and activated carbon (AC) for polysulfide immobilization to form a stable and uniform scaffold to host S in Li-S batteries for energy storage. On one hand,  $\text{NiFe}_2\text{O}_4$  nanoparticles have limited chemical sites for adsorption of polysulfides and electrocatalytic transformation of polysulfides. On the other hand, the AC network structure possesses high conductivity, which ensures the rapid transmission of electrons within the electrode and prevents the agglomeration of  $\text{NiFe}_2\text{O}_4$  nanoparticles and sulfur. The AC- $\text{NiFe}_2\text{O}_4$ /S composite with a high sulfur content ( $\sim 61\%$ ; sulfur loading of  $\sim 1.5 \text{ mg cm}^{-2}$ ) achieves specific capacities of  $\sim 600$  and  $500 \text{ mAh g}^{-1}$  at 0.1 and 0.5 C, respectively, with excellent Coulombic efficiency (nearly 98%) and cycle stability with a fade rate as low as  $\sim 0.24\%$  per cycle.

## 2. EXPERIMENTAL SECTION

### 2.1. Materials and characterization methods

All chemicals used as received without further purification.  $\text{Fe}(\text{NO}_3)_3 \cdot 9\text{H}_2\text{O}$ ,  $\text{Ni}(\text{NO}_3)_2 \cdot 6\text{H}_2\text{O}$ , sodium hydroxide (NaOH), AC, and sublimed sulfur were purchased from Aladdin. Crystalline phases were characterized using X-ray diffraction (XRD; D8-Advance, Germany) with Cu K $\alpha$  radiation ( $\lambda = 1.5406 \text{ \AA}$ , 40 kV, 40 mA). The morphology and structure of the materials was characterized by scanning electron microscopy (SEM; FEI QUANTA FEG 450) at 20 kV. Transmission electron microscopy (TEM) was performed on an electron microscope Talos F200X, FEI, USA).  $\text{N}_2$  adsorption/desorption analysis was conducted on an Autosorb-iQ2 analyzer (Quantachrome Instruments) that was equipped with a liquid  $\text{N}_2$  bath to keep the temperature at 77 K.

## 2.2. Synthesis of $\text{NiFe}_2\text{O}_4$ and AC- $\text{NiFe}_2\text{O}_4$ binary host

To prepare  $\text{NiFe}_2\text{O}_4$ ,  $\text{Fe}(\text{NO}_3)_3 \cdot 9\text{H}_2\text{O}$  (10 mmol) and  $\text{Ni}(\text{NO}_3)_2 \cdot 6\text{H}_2\text{O}$  (5 mmol) were dispersed in deionized water (200 mL) by vigorous stirring. NaOH was added. The obtained Ni-Fe double hydroxide was collected by centrifugation and then washed with deionized water. The obtained powder was dried and then annealed at 800 °C for 2 h under an air atmosphere to produce  $\text{NiFe}_2\text{O}_4$ .

To prepare AC- $\text{NiFe}_2\text{O}_4$ , AC (60 mg) and  $\text{NiFe}_2\text{O}_4$  (8 mg) were dispersed in a mixture of deionized water (60 mL) and absolute ethanol (20 mL) by sonication for 30 min. The mixture was transferred to a 100-mL Teflon-lined stainless-steel autoclave and subjected to solvothermal reaction at 180 °C for 12 h. The solid product was collected by centrifugation, washed with distilled water and ethanol several times, and then dried.

## 2.3. Synthesis of the AC- $\text{NiFe}_2\text{O}_4/\text{S}$ composite

To synthesize the AC- $\text{NiFe}_2\text{O}_4/\text{S}$  composite, AC- $\text{NiFe}_2\text{O}_4$  (50 mg) and sulfur powder to give a mass ratio of 3:1 were ground together using a typical melt-diffusion approach. The mixture was transferred to a sealed Teflon reactor filled with Ar and heated at 155 °C for 10 h and then 250 °C for 20 min. As a control, an AC/S composite was prepared by the same method using AC instead of AC- $\text{NiFe}_2\text{O}_4$ .

## 2.4 Electrochemical measurements

Electrochemical measurements were performed in a two-electrode half coin cell. AC- $\text{NiFe}_2\text{O}_4/\text{S}$ , Super P, and polyvinylidene fluoride (PVDF) with a weight ratio of 80:10:10 were dissolved in N-methyl-2-pyrrolidone (NMP) and then pasted onto aluminum foil as a current collector. The average sulfur mass loading density was between 1.4 and 1.6 mg  $\text{cm}^{-2}$ . Each coin cell (2032 type) was assembled using lithium foil as the anode, a Celgard 2400 sheet as the separator, and electrolyte consisting of 1 M lithium bis(trifluoromethanesulfonyl)imide (LiTFSI) in a mixture of DOL/DME (1:1 v/v) with 1 wt %  $\text{LiNO}_3$  in a high-purity argon-filled glove box with moisture and oxygen concentrations below 1 ppm. Galvanostatic charge-discharge performance was measured using a battery tester (BTS3000, Neware, China) between 2.8 and 1.7 V (vs.  $\text{Li}/\text{Li}^+$ ) at current densities based on the weight of sulfur (1 C = 1675 mA  $\text{g}^{-1}$ ) at room temperature (25 °C).

# 3. RESULTS AND DISCUSSION

## 3.1. Morphological and structural characterization

To obtain AC- $\text{NiFe}_2\text{O}_4$  host materials, first,  $\text{NiFe}_2\text{O}_4$  was prepared by calcination.  $\text{NiFe}_2\text{O}_4$  was transformed into AC- $\text{NiFe}_2\text{O}_4$  by a solvothermal process. Finally, the AC- $\text{NiFe}_2\text{O}_4/\text{S}$  cathode material was obtained after impregnating sulfur into the AC- $\text{NiFe}_2\text{O}_4$  material. Figure 1a displays the synthesis

process of the AC–NiFe<sub>2</sub>O<sub>4</sub>/S composite. The porous AC acts as a support for the NiFe<sub>2</sub>O<sub>4</sub> nanocrystals and enhances electron conduction to facilitate electrochemical reactions.

The morphologies of AC (Fig. 2b and c) and AC–NiFe<sub>2</sub>O<sub>4</sub>/S (Fig. 2a and d) were observed by SEM. The SEM analysis revealed the 3D porous and hierarchical structure of the AC–NiFe<sub>2</sub>O<sub>4</sub>/S composite. NiFe<sub>2</sub>O<sub>4</sub> nanoparticles were tightly anchored on the AC along with S to form a conductive and robust 3D framework. Compared with the case for the AC–NiFe<sub>2</sub>O<sub>4</sub> composite, there is no superficial attachment of AC–NiFe<sub>2</sub>O<sub>4</sub> when it is loaded with sulfur. The strong fusion of sulfur and AC ensured that sulfur was successfully loaded into the mixed pores of AC–NiFe<sub>2</sub>O<sub>4</sub>.

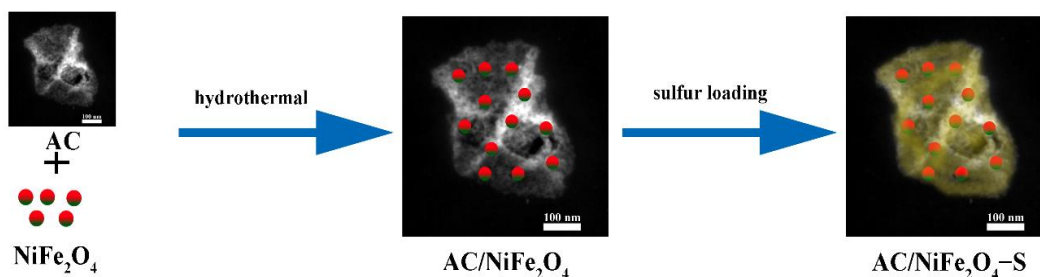


**Figure 1.** Schematic illustration of the synthesis process of AC–NiFe<sub>2</sub>O<sub>4</sub>/S.

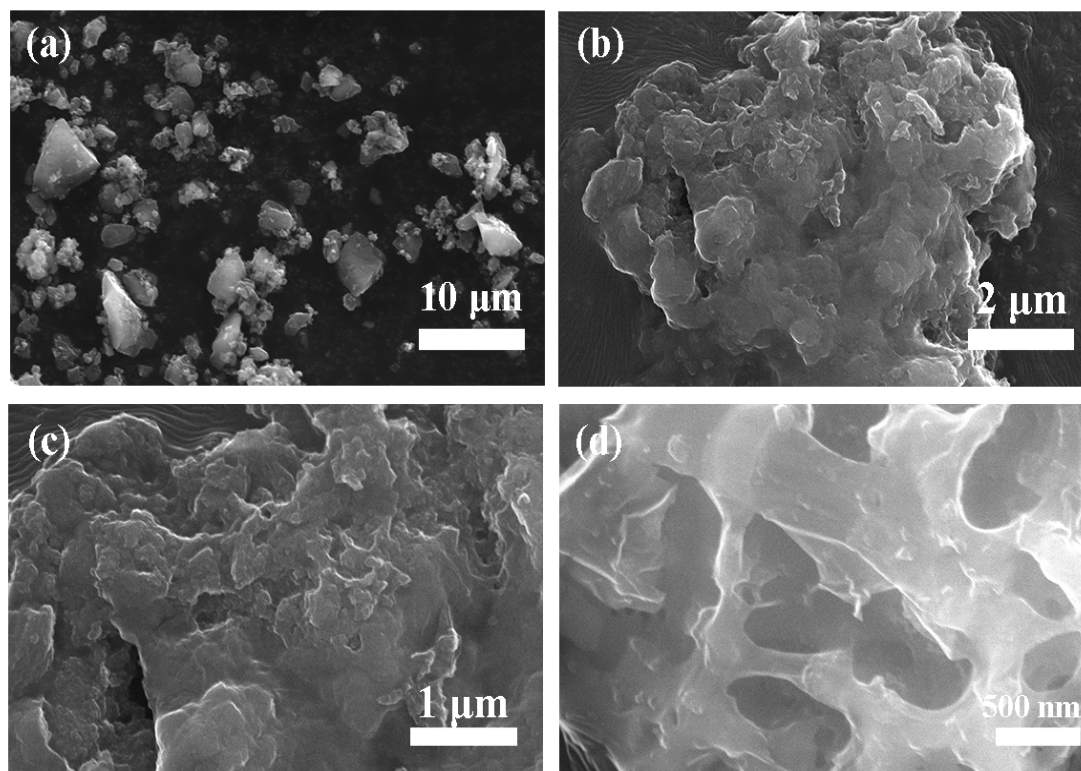


**Figure 2.** SEM images of the (b, c) AC–NiFe<sub>2</sub>O<sub>4</sub> and (a, d) AC–NiFe<sub>2</sub>O<sub>4</sub>/S composites.

XRD patterns of AC, NiFe<sub>2</sub>O<sub>4</sub>, AC–NiFe<sub>2</sub>O<sub>4</sub>, and AC–NiFe<sub>2</sub>O<sub>4</sub>/S are shown in Figure 3a. The AC–NiFe<sub>2</sub>O<sub>4</sub> composite exhibited several diffraction peaks that were ascribed to cubic NiFe<sub>2</sub>O<sub>4</sub> (JCPDS #54-0964). The broadening of the diffraction peaks indicates the small size of the NiFe<sub>2</sub>O<sub>4</sub> nanocrystals. The XRD pattern of the AC–NiFe<sub>2</sub>O<sub>4</sub>/S composite (Figure 3a) showed a series of peaks derived from orthorhombic  $\alpha$ -S<sub>8</sub> (JCPDS No. 78-1888), indicating that S was incorporated into the AC–NiFe<sub>2</sub>O<sub>4</sub> host. Thermogravimetric analysis (TGA) showed that the sulfur content of the AC–NiFe<sub>2</sub>O<sub>4</sub>/S composite was approximately 61.5 wt% (Fig. 3b).

Nitrogen adsorption-desorption isotherms confirmed that sulfur was successfully incorporated into the AC–NiFe<sub>2</sub>O<sub>4</sub>/S composite (Figure 3c). AC–NiFe<sub>2</sub>O<sub>4</sub> exhibited a typical type-III isotherm with substantial H<sub>2</sub> hysteresis, indicating the coexistence of micropores and mesopores based on the IUPAC classification [25]. The main mesoporous structure of AC–NiFe<sub>2</sub>O<sub>4</sub> was verified and its Brunauer–Emmett–Teller (BET) surface area was as high as 1196.4 m<sup>2</sup> g<sup>-1</sup> and its pore volume was 0.89 cm<sup>3</sup> g<sup>-1</sup>. In contrast, after the inclusion of sulfur, the BET surface area of the AC–NiFe<sub>2</sub>O<sub>4</sub>/S composite material decreased markedly to 51.1 m<sup>2</sup> g<sup>-1</sup> and its pore volume was only 0.08 cm<sup>3</sup> g<sup>-1</sup>, indicating successful loading of sulfur into the host material.

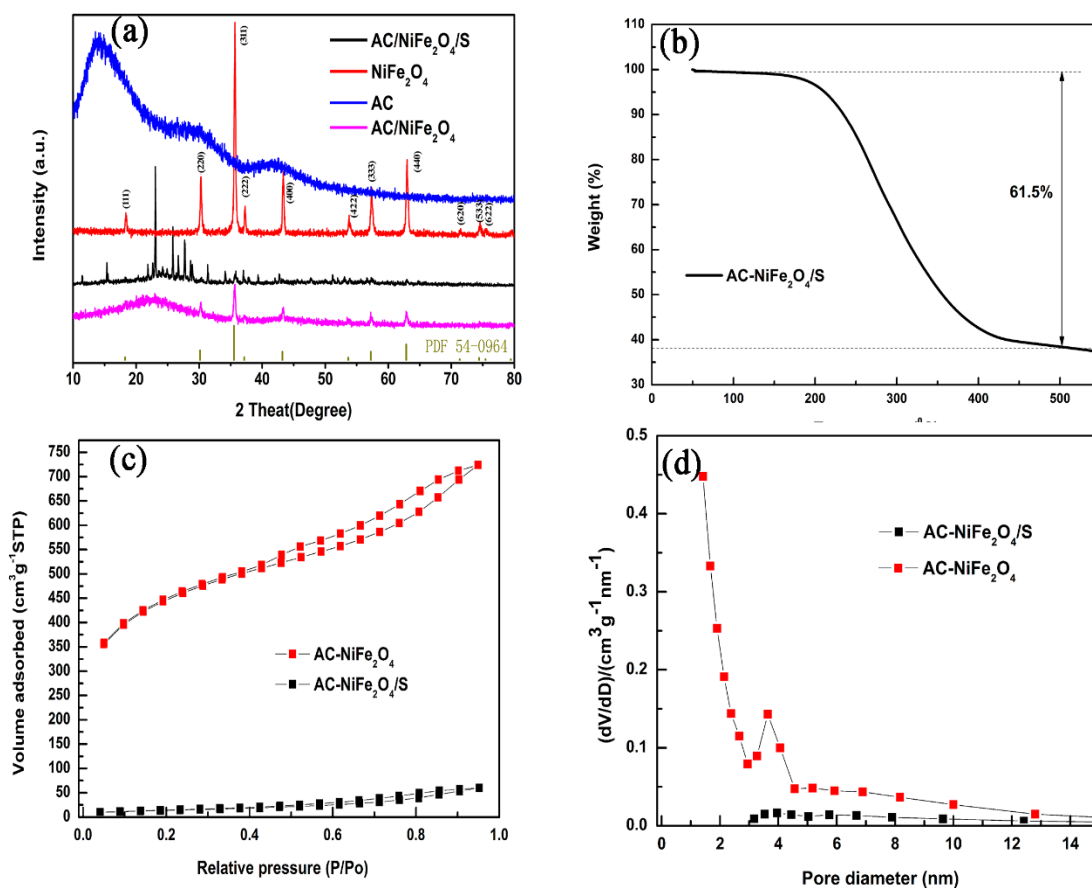


**Figure 3.** (a) XRD patterns showing the phase compositions of AC, NiFe<sub>2</sub>O<sub>4</sub>, AC–NiFe<sub>2</sub>O<sub>4</sub>, and AC–NiFe<sub>2</sub>O<sub>4</sub>/S. (b) TGA plots, (c) nitrogen adsorption–desorption isotherms, and (d) pore size distributions of AC–NiFe<sub>2</sub>O<sub>4</sub> and AC–NiFe<sub>2</sub>O<sub>4</sub>/S.

TEM analysis (Fig. 4) of the AC–NiFe<sub>2</sub>O<sub>4</sub>/S composite confirmed that NiFe<sub>2</sub>O<sub>4</sub> nanocrystals were uniformly distributed on AC and AC was entangled with S, consistent with SEM observations (Fig. 2d). The TEM image in Fig. 4a shows that the S particles are well encapsulated in the AC–NiFe<sub>2</sub>O<sub>4</sub> framework, confirming successful sulfur immobilization. The TEM image also indicates that the NiFe<sub>2</sub>O<sub>4</sub> nanoparticles are well preserved after sulfur loading. The energy-dispersive X-ray spectroscopy (EDS) results (Fig. 4) indicated the presence of S, C, Fe, Ni, and O in the cathode material. Sulfur was uniformly distributed in the AC–NiFe<sub>2</sub>O<sub>4</sub> bulk, further confirming the successful loading of sulfur. The AC–NiFe<sub>2</sub>O<sub>4</sub>/S cathode material ensures intimate contact between S and the NiFe<sub>2</sub>O<sub>4</sub> nanocrystals, which should allow formation of a multifunctional adsorption/conversion interface for the polysulfide redox reaction.

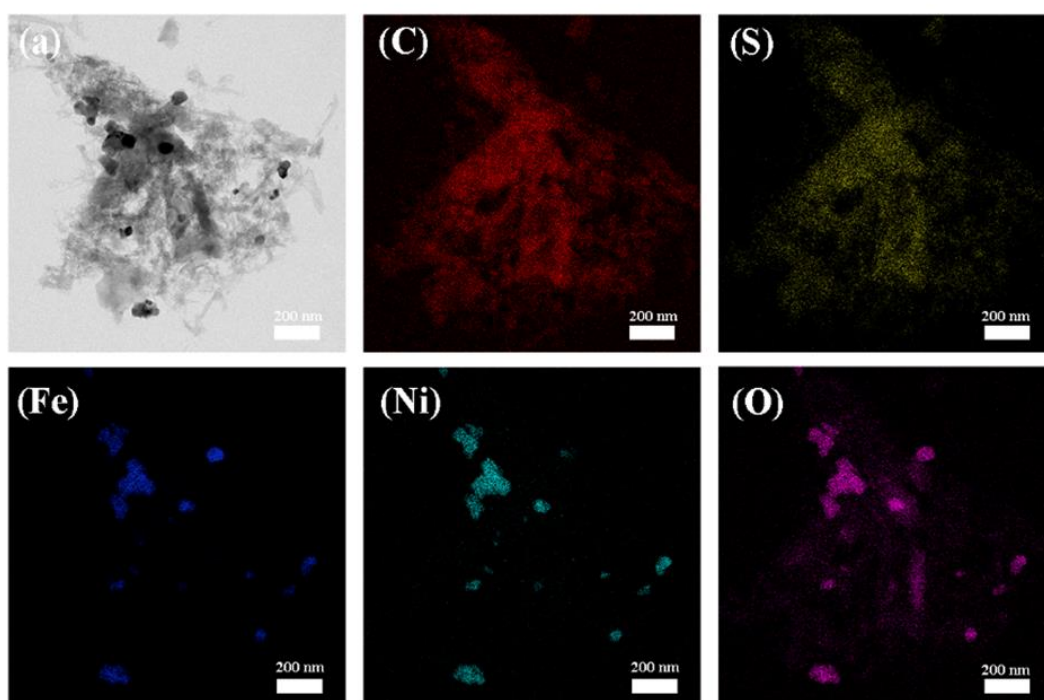


**Figure 4.** (a) TEM image of AC–NiFe<sub>2</sub>O<sub>4</sub>/S and corresponding EDS mapping images of C, S, Fe, Ni, O, and S.

### 3.2. Electrochemical properties

The electrochemical performance of the AC–NiFe<sub>2</sub>O<sub>4</sub>/S composite was measured using coin cells to reveal the role of NiFe<sub>2</sub>O<sub>4</sub> nanocrystals. The sulfur loading of both AC/S and AC–NiFe<sub>2</sub>O<sub>4</sub>/S electrodes was approximately 1.5 mg cm<sup>-2</sup>. Electrochemical impedance spectroscopy (EIS) over the frequency range from 0.1 Hz to 100 kHz at a scan rate of 0.1 mV s<sup>-1</sup> showed that the AC–NiFe<sub>2</sub>O<sub>4</sub>/S composite electrode had a much lower charge transfer resistance ( $R_{ct}$ ) than that of the AC/S composite (Fig. 5a). This result indicates that the NiFe<sub>2</sub>O<sub>4</sub> nanocrystals in AC–NiFe<sub>2</sub>O<sub>4</sub> accelerate the charge transfer kinetics at the polysulfide interface because of the markedly enhanced redox kinetics of polysulfides on AC–NiFe<sub>2</sub>O<sub>4</sub>/S compared with that on AC–NiFe<sub>2</sub>O<sub>4</sub>/S.

Figure 5b shows typical cyclic voltammetry (CV) curves for the first three cycles of the AC–NiFe<sub>2</sub>O<sub>4</sub>/S electrode at a scan rate of 0.1 mV s<sup>-1</sup>. The initial CV curve contained two cathodic peaks at 2.3 and 2.06 V related to the conversion of orthorhombic sulfur (S<sub>8</sub>) into soluble lithium polysulfide Li<sub>2</sub>S<sub>x</sub> (4 ≤ x ≤ 8) and then into insoluble sulfides (Li<sub>2</sub>S<sub>2</sub>/Li<sub>2</sub>S), respectively [26, 27].

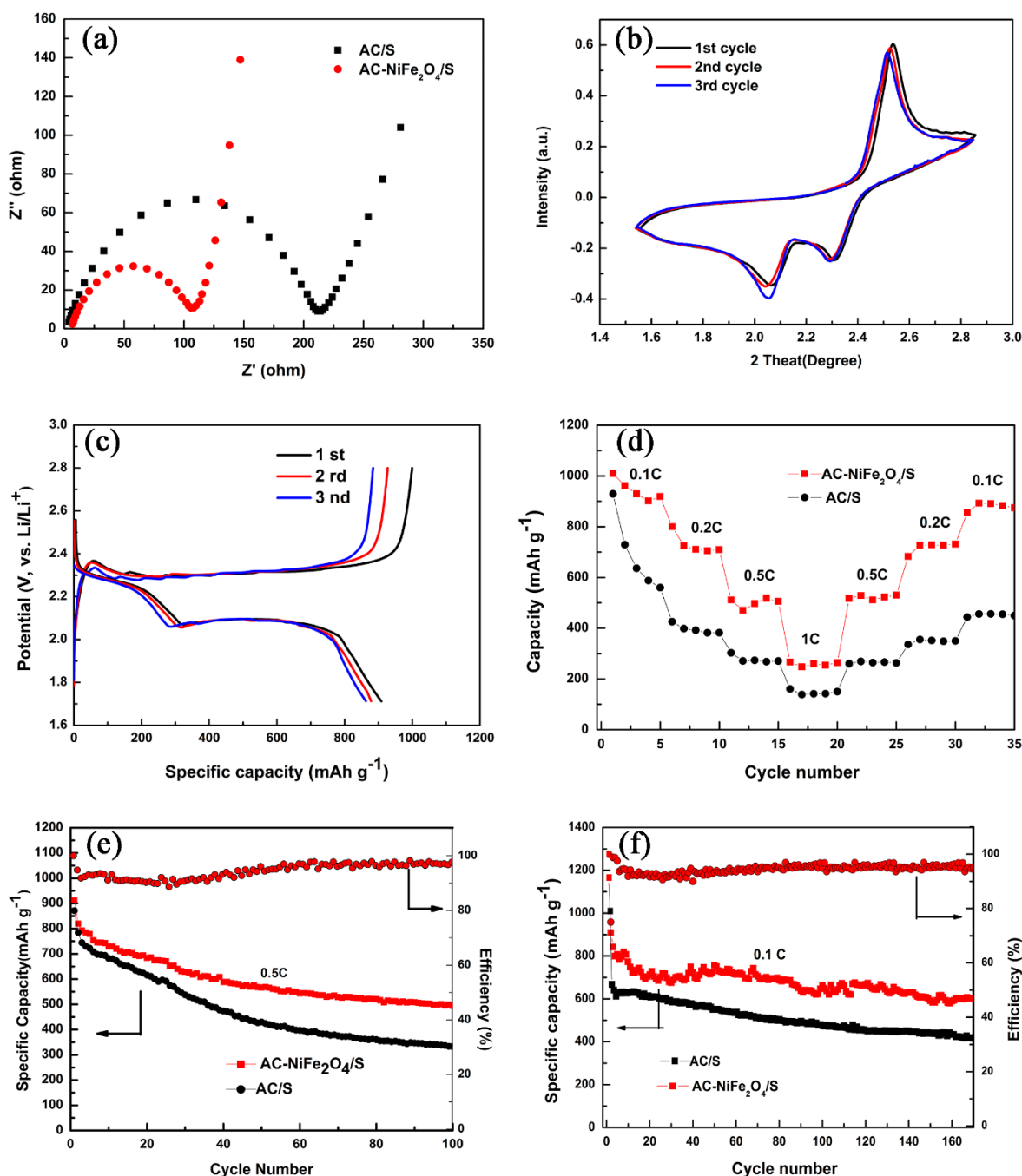


**Figure 5.** Electrochemical performance of the AC–NiFe<sub>2</sub>O<sub>4</sub>/S cathode. (a) EIS data recorded before cycling. (b) CV curves of AC–NiFe<sub>2</sub>O<sub>4</sub>/S at a scan rate of 0.1 mV s<sup>-1</sup>. (c) Galvanostatic charge–discharge profiles in the first, second, and third cycles at a rate of 0.1 C. (d) Rate performance. (e) Cycling performance and Coulombic efficiency at 0.5 C. (f) Long-term cycling performance and Coulombic efficiency at a rate of 1 C.

In the subsequent anodic scan, the oxidation peak at 2.51 V corresponded to reversible stepwise reoxidation of  $\text{Li}_2\text{S}/\text{Li}_2\text{S}_2$  to sulfur [28]. In the first three cycles, no obvious shifts of peak potential were observed for the AC– $\text{NiFe}_2\text{O}_4/\text{S}$  electrode, indicating its good electrochemical reversibility and stability. To evaluate the long-term cycling performance of the AC– $\text{NiFe}_2\text{O}_4/\text{S}$  hybrid material, the discharge–charge distribution of an AC– $\text{NiFe}_2\text{O}_4/\text{S}$  electrode at 0.1 C ( $1\text{C} = 1675 \text{ mAh g}^{-1}$ ) for 170 cycles was measured (Fig. 5b). The AC– $\text{NiFe}_2\text{O}_4/\text{S}$  composite exhibited high initial discharge and charge capacities of 994.5 and 908.7  $\text{mAh g}^{-1}$ , respectively. Figure 5c shows the cycle performance of the AC/S electrode at 0.1 C. The AC/S electrode exhibited an initial discharge capacity of 951.6  $\text{mAh g}^{-1}$  and a low capacity of 416.1  $\text{mAh g}^{-1}$  after 170 cycles. In contrast, the AC– $\text{NiFe}_2\text{O}_4/\text{S}$  electrode achieved a high discharge capacity of 602.7  $\text{mAh g}^{-1}$  with a Coulombic efficiency of 98% throughout the 170th cycle, which gave a higher capacity retention of 60% (0.24% capacity decay per cycle). This indicates that the incorporation of  $\text{NiFe}_2\text{O}_4$  nanocrystals effectively suppressed the dissolution of polysulfides in the organic electrolyte.

Figure 5d presents the rate performance of AC/S and AC– $\text{NiFe}_2\text{O}_4/\text{S}$  cathodes at various current rates from 0.1 to 1.0 C. The AC– $\text{NiFe}_2\text{O}_4/\text{S}$  cathode displayed obviously better rate performance than that of the AC/S cathode. At 0.1, 0.2, 0.5, and 1.0 C, the capacities of the AC– $\text{NiFe}_2\text{O}_4/\text{S}$  electrode were 1009.6, 804.8, 514.2, and 273.1  $\text{mAh g}^{-1}$ , respectively, whereas those for the AC–S cathode decreased to 908.1, 403.7, 301.2, and 149.5  $\text{mAh g}^{-1}$ , respectively. In addition, the cycling performance of the electrodes at a rate of 0.5 C was also studied (Fig. 5g). The AC– $\text{NiFe}_2\text{O}_4/\text{S}$  electrode showed a high capacity of 501.9  $\text{mA h g}^{-1}$  after 100 cycles, which is equivalent to a capacity retention of 55.2% (0.44% capacity decay per cycle). In contrast, the AC/S electrode showed a much lower capacity of 332.1  $\text{mAh g}^{-1}$  after 100 cycles at 0.5 C. The Coulombic efficiency of the AC– $\text{NiFe}_2\text{O}_4/\text{S}$  electrode was maintained at around 98% during long-term cycling. Table 1 tabulates numeric comparisons of the cell performance based on various carbon-sulfur composite cathodes.

**Table 1.** Cell performance based on carbon-sulfur composite cathodes.

Cathode material	Initial capacity ( $\text{mA h g}^{-1}$ )	Capacity retention ( $\text{mA h g}^{-1}$ )	Cycle number	Rate	Sulfur amount	Ref.
PEG–MC/S	1290	520	40	0.03C	20wt%	29
MC/S	1083	200	50	0.12C	67wt%	30
m-MC/S	1000	600	800	1C	40wt%	31
CNT/S	655	670	60	0.06C	68wt%	32
pPAN–CNT/S	820	697	50	0.1C	63wt%	33
Hollow CNT/S	~1500	660	100	0.25C	40wt%	34
rGO/S	~810	~576	100	0.3C	40wt%	35
G/S	1068	~450	80	0.1C	66wt%	36
AC– $\text{NiFe}_2\text{O}_4/\text{S}$	1170	~600	170	0.1C	61wt%	This work

#### 4. CONCLUSIONS

We developed a facile and scalable method to produce an AC–NiFe<sub>2</sub>O<sub>4</sub>/S hybrid material that uses porous AC as electron and lithium-ion diffusion pathways. The NiFe<sub>2</sub>O<sub>4</sub> nanoparticles of AC–NiFe<sub>2</sub>O<sub>4</sub>/S addressed polysulfide dissolution/shuttling problems, regulating their conversion and promoting Li<sub>2</sub>S deposition to enhance the performance of Li–S batteries. The AC–NiFe<sub>2</sub>O<sub>4</sub>/S cathode displayed stable electrochemical performance, exhibiting a low capacity decay rate and high coulombic efficiency. After 170 cycles, its capacity decayed by only 0.24% per cycle and its reversible capacity remained at 602.7 mAh g<sup>-1</sup>. Even though only 1.5 mg cm<sup>-2</sup> of S was loaded into the AC–NiFe<sub>2</sub>O<sub>4</sub>/S cathode, the corresponding battery maintained a relatively high energy density of 501.9 mAh g<sup>-1</sup> after 100 cycles at 0.5 C. Our test results showed that AC could not only provide a large surface area and high pore volume to load S, but also accelerated electron conduction. Meanwhile, NiFe<sub>2</sub>O<sub>4</sub> acted as an electrocatalyst to promote the conversion of lithium polysulfides. Overall, this work demonstrated that AC–NiFe<sub>2</sub>O<sub>4</sub>/S can improve the specific capacity and cycling stability of Li–S batteries.

#### ACKNOWLEDGEMENTS

The authors gratefully acknowledge support from the National Natural Science Foundation of China (5187011196, U1501242 and 51671062), National Key Research and Development Program (2018YFB1502103, 2018YFB1502105), Guangxi Bagui Scholar Foundation, Guangxi Collaborative Innovation Centre of Structure and Property for New Energy and Materials (2012GXNSFGA06002), Guangxi Science and Technology Project (AD17195073, 2017AD23029), and Guangxi Major Science and Technology Special Project (AA17202030-1). We also thank the Guangxi Advanced Functional Materials Foundation and Application Talents Small Highlands, and the Innovation Project of Guangxi Graduate Education (2019YCX112), for providing financial support. F.R. is grateful to the Canada Research Chairs program for partial salary support.

#### References

1. X. Tao, J. Wang, C. Liu, H. Wang, H. Yao, G. Zheng, Z. W. Seh, Q. Cai, W. Li, G. Zhou, C. Zu, and Y. Cui, *Nat. Commun.*, 7(2016) 11203.
2. T. Chen, B. Cheng, G. Zhu, R. Chen, Y. Hu, L. Ma, H. Lv, Y. Wang, J. Liang, Z. Tie, Z. Jin, and J. Liu, *Nano Lett.*, 17(2017) 437.
3. K. Wang, L.-j. Cheng, J.-g. Zhang, and X.-b. Yu, *Int. J. Hydrogen Energy*, 43(2018) 4177.
4. C.-C. Xu, Y. Wang, L. Li, Y.-J. Wang, L.-F. Jiao, and H.-T. Yuan, *Rare Met.*, 38(2015) 29.
5. J. H. Kim, K. Fu, J. Choi, K. Kil, J. Kim, X. Han, L. Hu, and U. Paik, *Sci. Rep.*, 5(2015) 8946.
6. Y. Hwa, J. Zhao, and E. J. Cairns, *Nano Lett.*, 15(2015) 3479.
7. S. Zhang, K. Ueno, K. Dokko, and M. Watanabe, *Adv. Energy Mater.*, 5(2015) 1500117.
8. H. S. Ryu, Z. Guo, H. J. Ahn, G. B. Cho, and H. Liu, *J. Power Sources*, 189(2009) 1179.
9. S. Choudhury, D. Fischer, P. Formanek, M. Stamm, and L. Ionov, *Adv. Mater. Interfaces*, 5(2018) 1701116.
10. Q. Fan, W. Liu, Z. Weng, Y. Sun, and H. Wang, *J. Am. Chem. Soc.*, 137(2015) 12946.
11. C. Wang, W. Wan, J.-T. Chen, H.-H. Zhou, X.-X. Zhang, L.-X. Yuan, and Y.-H. Huang, *J. Mater. Chem. A*, 1(2013) 1716.

12. F. Sun, J. Wang, D. Long, W. Qiao, L. Ling, C. Lv, and R. Cai, *J. Mater. Chem. A*, 1(2013).13283
13. C. Zhang, Z. Zhang, D. Wang, F. Yin, and Y. Zhang, *J. Alloys Compd.*, 714(2017) 126.
14. Y. Xiao, C. Long, M.-T. Zheng, H.-W. Dong, B.-F. Lei, H.-R. Zhang, and Y.-L. Liu, *Chin. Chem. Lett.*, 25(2014) 865.
15. L. Chen, H. Zhou, C. Fu, Z. Chen, C. Xu, and Y. Kuang, *Int. J. Hydrogen Energy*, 41(2016) 21850.
16. Y. Zhou, C. Zhou, Q. Li, C. Yan, B. Han, K. Xia, Q. Gao, and J. Wu, *Adv. Mater.*, 27(2015) 3774.
17. Q. Zhang, Y. Wang, Z. W. Seh, Z. Fu, R. Zhang, and Y. Cui, *Nano Lett.*, 15(2015) 3780.
18. Z. Xiao, Z. Yang, L. Wang, H. Nie, M. Zhong, Q. Lai, X. Xu, L. Zhang, and S. Huang, *Adv. Mater.*, 27(2015) 2891.
19. X. Liang, C. Hart, Q. Pang, A. Garsuch, T. Weiss, and L. F. Nazar, *Nat. Commun.*, 6(2015) 5682.
20. C. J. Hart, M. Cuisinier, X. Liang, D. Kundu, A. Garsuch, and L. F. Nazar, *Chem. Commun.*, 51(2015) 2308.
21. Z. Zhang, L.-L. Kong, S. Liu, G.-R. Li, and X.-P. Gao, *Adv. Energy Mater.*, 7(2017).
22. Z. Cui, C. Zu, W. Zhou, A. Manthiram, and J. B. Goodenough, *Adv. Mater.*, 28(2016) 6926.
23. J. Cheng, D. Zhao, L. Fan, X. Wu, M. Wang, N. Zhang, and K. Sun, *J. Mater. Chem. A*, 5(2017) 14519.
24. W. Bao, D. Su, W. Zhang, X. Guo, and G. Wang, *Adv. Funct. Mater.*, 26(2016) 8746.
25. H. J. Peng, Z. W. Zhang, J. Q. Huang, G. Zhang, J. Xie, W. T. Xu, J. L. Shi, X. Chen, X. B. Cheng, and Q. Zhang, *Adv. Mater.*, 28(2016) 9551.
26. G. Li, J. Sun, W. Hou, S. Jiang, Y. Huang, and J. Geng, *Nat. Commun.*, 7(2016) 10601.
27. L. Luo and A. Manthiram, *ACS Energy Lett.*, 2(2017) 2205.
28. W. Bao, L. Liu, C. Wang, S. Choi, D. Wang, and G. Wang, *Adv. Energy Mater.*, 8(2018) .
29. C. Zhang, W. Lv, W. Zhang, X. Zheng, M.-B. Wu, W. Wei, Y. Tao, Z. Li, and Q.-H. Yang, *Adv. Energy Mater.*, 4(2014) 1301565.
30. L. Yuan, H. Yuan, X. Qiu, L. Chen, and W. Zhu, *J. Power Sources*, 189(2009) 1141.
31. L. Yin, J. Wang, J. Yang, and Y. Nuli, *J. Mater. Chem.*, 21(2011) 6807.
32. H. Ye, Y.-X. Yin, S. Xin, and Y.-G. Guo, *J. Mater. Chem. A*, 1(2013) 6602.
33. J. Wang, Y. Wu, Z. Shi, and C. Wu, *Electrochim. Acta*, 144(2014) 307.
34. J. Wang, S. Y. Chew, Z. W. Zhao, S. Ashraf, D. Wexler, J. Chen, S. H. Ng, S. L. Chou, and H. K. Liu, *Carbon*, 46(2008) 229.
35. J. Guo, Y. Xu, and C. Wang, *Nano Lett.*, 11(2011) 4288.
36. J.-Q. Huang, X.-F. Liu, Q. Zhang, C.-M. Chen, M.-Q. Zhao, S.-M. Zhang, W. Zhu, W.-Z. Qian, F. Wei, *Nano Energy*, 2(2013) 314.